Journal of ELECTRONIC MATERIALS, Vol. 47, No. 2, 2018
DOI: 10.1007/s11664-017-5937-3
© 2017 The Minerals, Metals & Materials Society

CrossMark

TOPICAL COLLECTION: 59TH ELECTRONIC MATERIALS CONFERENCE 2017

Metalorganic Vapor-Phase Epitaxy Growth Parameters for Two-Dimensional MoS_2

M. MARX,[1,4] A. GRUNDMANN,[1] Y.-R. LIN,[2] D. ANDRZEJEWSKI,[3] T. KÜMMELL,[3] G. BACHER,[3] M. HEUKEN,[1,2] H. KALISCH,[1] and A. VESCAN[1]

1.—GaN Device Technology, RWTH Aachen University, Sommerfeldstr. 24, 52074 Aachen, Germany. 2.—AIXTRON SE, Dornkaulstr. 2, 52134 Herzogenrath, Germany. 3.—Werkstoffe der Elektrotechnik and CENIDE, University Duisburg-Essen, Bismarckstraße 81, 47057 Duisburg, Germany. 4.—e-mail: marx@gan.rwth-aachen.de

The influence of the main growth parameters on the growth mechanism and film formation processes during metalorganic vapor-phase epitaxy (MOVPE) of two-dimensional MoS_2 on sapphire (0001) have been investigated. Deposition was performed using molybdenum hexacarbonyl and di-*tert*-butyl sulfide as metalorganic precursors in a horizontal hot-wall MOVPE reactor from AIXTRON. The structural properties of the MoS_2 films were analyzed by atomic force microscopy, scanning electron microscopy, and Raman spectroscopy. It was found that a substrate prebake step prior to growth reduced the nucleation density of the polycrystalline film. Simultaneously, the size of the MoS_2 domains increased and the formation of parasitic carbonaceous film was suppressed. Additionally, the influence of growth parameters such as reactor pressure and surface temperature is discussed. An upper limit for these parameters was found, beyond which strong parasitic deposition or incorporation of carbon into MoS_2 took place. This carbon contamination became significant at reactor pressure above 100 hPa and temperature above 900°C.

Key words: MOVPE, MOCVD, 2D materials, MoS_2

INTRODUCTION

Layered transition-metal dichalcogenides (TMDC) have attracted a lot of attention in the research field of two-dimensional (2D) materials. The electrical behavior of the class of 2D TMDC varies from metallic (NbS_2) to semiconducting with direct bandgaps between 1.1 eV ($MoTe_2$)[1] and 1.94 eV (WS_2).[2] The basal plane of TMDC consists of a hexagonally packed lattice plane of a transition metal between two layers of chalcogen atoms.[3] Despite having thickness of only three atoms, the monolayer is thermodynamically stable and has outstanding mechanical properties.[4] The bonds between the basal-plane monolayers are of van der Waals type, whereas the internal ones are covalent. Due to the absence of dangling bonds in the out-of-plane direction, it is expected that heterostructures including these materials will have less constraints regarding lattice mismatch and feature lower interface trap densities.[5] Along with their unique optical properties, TMDC are very interesting for scientific research and could find application in numerous electronic and optoelectronic devices.

However, one major challenge remains reproducible and homogeneous fabrication of 2D TMDC on wafer scale. One promising technique in this regard is metalorganic vapor-phase epitaxy (MOVPE), which is based on established, state-of-the-art tools. However, there have been few reports on MOVPE of 2D TMDC to date.[6–10] Deposition of polycrystalline 2D MoS_2 on wafer scale with domain sizes on the micrometer scale was demonstrated by Kang et al.[8] Intensive research has also been

(Received June 27, 2017; accepted November 7, 2017; published online November 22, 2017)

performed on growth of 2D WSe_2.[7] Nevertheless, the processes used in these studies differ fundamentally in terms of precursor chemistry and growth conditions; For example, Kang et al. used diethyl sulfide (DES),[8] Eichfeld et al. applied dimethyl selenide (DMSe),[7] whereas our group used di-*tert*-butyl sulfide (DTBS),[6] which all have distinct organic groups and thus different dissociation and growth properties. In some cases, similar approaches have even led to contrary results; For example, Eichfeld et al. reported successful growth in pure H_2 atmosphere,[7] while Kang et al. (and our group) observed a strong etching effect of H_2 during growth.[6,8] In addition, while Eichfeld and our group deposited TMDC at high temperature (800°C to 900°C), Kang et al. chose low temperatures (550°C). In summary, it is obvious that the optimum conditions for the growth process are still not sufficiently understood.

Therefore, we started to thoroughly investigate the growth of 2D MoS_2 via MOVPE. In this work, we focus on thermal pretreatment of the sapphire substrate as well as the influence of the reactor pressure and growth temperature on the morphology of the deposited films.

EXPERIMENTAL PROCEDURES

Experiments were carried out in an AIXTRON horizontal hot-wall MOVPE reactor in a 10 × 2 inch configuration. As Mo source, molybdenum hexacarbonyl (MCO) with 99.9% purity was chosen. In this compound, the Mo atom has valence of zero, hence thermal decomposition of MCO via decarbonylation starts at low temperatures (> 150°C). Additionally, the split-off carbonyl group forms a stable noncondensing gas (carbon monoxide), which minimizes parasitic carbon incorporation into the growing crystal. The MCO source is kept at 0°C, resulting in vapor pressure of 1.1 Pa.[11] Di-*tert*-butyl sulfide (DTBS, 99.999%), used as the sulfur source, has long been applied for MOVPE processes. In comparison with H_2S, DTBS offers the advantages that parasitic prereactions in the gas phase are less of an issue and that it is nontoxic.[12,13] According to its material data sheet, vapor pressure of 5.22 hPa is established when maintaining the source at 17°C. The precursor flows were set to 0.1 nmol/min for MCO and to 20 μmol/min for DTBS in all experiments (S/Mo ratio 200,000). Such high ratio is necessary to obtain a 2D growth mode and to allow investigation of the nucleation process.[7,8] In this work, we focused on deposition on sapphire (0001) substrates with nominal offcut of 0.2° towards m-plane. Their a-lattice constant of 0.476 nm is approximately 1.5 times higher than the lattice constant of MoS_2 (0.315 nm).[14] It has been shown that this combination leads to a 3-on-2 structure as well as defined crystal alignment and orientation of MoS_2 on sapphire substrates.[15] The energetically favored orientation results in grain boundaries with partially metallic behavior. Conductivity inhomogeneities due to grain boundaries can thus be reduced when using such an orientation.[15,16] This will also be beneficial for fabrication of electrical devices consisting of polycrystalline material.

In our first series of experiments, we investigated the influence of thermal pretreatment (prebake) of the sapphire substrate on the later MoS_2 nucleation. Prebakes prior to growth are commonly used for conditioning substrates in MOVPE processes. The aim is to heal residual subsurface damage, remove contamination from the substrate via a polishing process, and establish reproducible surface conditions for MOVPE. For the first series of experiments, a standard nucleation step of MoS_2 on sapphire substrates was carried out after prebaking at various temperatures (850°C, 1050°C, and 1150°C), in different atmospheres (N_2 and H_2), and for different durations (15 min and 30 min). The standard nucleation process was carried out at 845°C and 30 hPa in pure N_2 atmosphere for 4 h. Residual H_2 from the prebake step can be excluded during the MoS_2 nucleation due to the low residence time ($\ll$ 1 min) and longer ramping step (5 min) to the growth conditions. In this work, the given temperatures are true temperatures, measured by emissivity-corrected pyrometry of the surface during growth. Metalorganic precursor flows were applied only during the growth steps but not in either the heating-up ramps or during the cooling-down phases.

In series 2, the influence of the reactor pressure parameter was investigated. The aim was to reduce the nucleation density to achieve a polycrystalline layer with low grain boundary density. Here, 6-h growth processes were performed after a 15-min prebake in H_2 at 1050°C. The growth temperature was kept at 845°C, while the reactor pressure was varied from 30 hPa to 400 hPa.

Finally, the results of the above series were combined into a two-step process with the intention of initiating MoS_2 nucleation in step 1 and focusing on lateral growth of existing crystallites in step 2. In step 1, growth was carried out at 845°C and 30 hPa for 4 h to obtain a defined nucleation density. In step 2 (6 h), the growth temperature was varied between 670°C and 1070°C to investigate the influence of temperature on lateral growth of MoS_2 nuclei.

The structural properties of the samples were characterized by Raman spectroscopy, atomic force microscopy (AFM), and scanning electron microscopy (SEM). The presented AFM and SEM images show characteristic sections of surface morphology, which can be similarly observed on the whole 2-inch substrate. The substrates were characterized by x-ray diffraction (XRD) analysis.

RESULTS

Figure 1a shows an SEM image of the surface of a MoS_2 sample deposited without any prebake. The small dark spots are 2D MoS_2 nucleation sites. The

typical triangular morphology of MoS_2 crystals can barely be resolved by SEM or AFM. The nucleation site density is very high, exceeding 550 nuclei/μm^2. The nuclei appear to be aligned along vertical lines with separation of about 55 nm. These lines are perpendicular to the substrate flat (substrate flat parallel to a- and perpendicular to m-plane). The origin of these lines are sapphire terraces. Their edges are monoatomic Al–Al steps with height h of 0.22 nm, formed due to the offcut α of the substrate.[17] The mean width w of a terrace can be estimated theoretically as

$$w = \frac{h}{\tan \alpha}. \quad (1)$$

The offcut of the substrates was individually measured using XRD and found to be 0.24° (nominal value 0.2° towards m-plane). Thus, the width of the terraces can be calculated to be 53 nm, in good agreement with the observed separation of the nucleation lines. As mentioned above, the orientation of the nucleation lines was parallel to the substrate flat, which matches the direction of the sapphire steps perpendicular to the m-plane. It can be concluded that nucleation of 2D MoS_2 takes place at sapphire terraces.

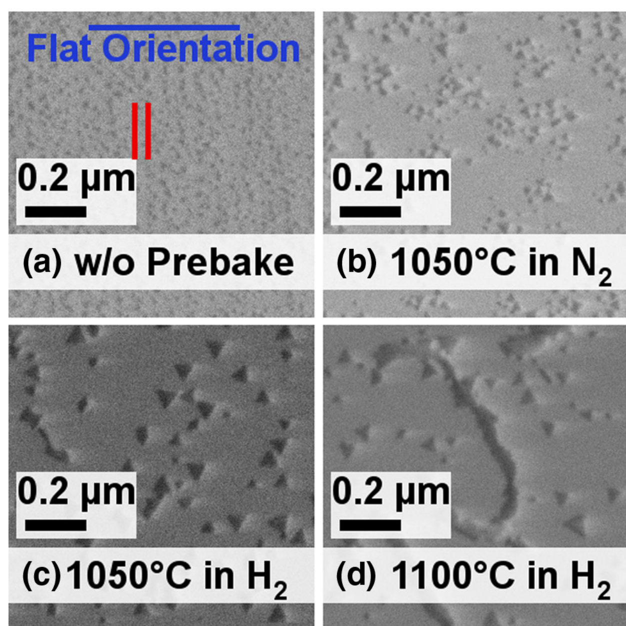

Fig. 1. SEM images of 2D MoS_2 nucleation sites deposited without and after different thermal substrate pretreatments. MoS_2 deposition was performed for each sample at 845°C and 30 hPa for 4 h. (a) Sample without prebake. The red lines illustrate two lines on which nucleation took place. The distance between the two lines is about 55 nm. (b) Sample with prebake at 1050°C in N_2 for 15 min. (c) Sample with the optimal prebake at 1050°C in H_2 for 15 min. (d) Sample with prebake at 1100°C in H_2 for 15 min. The sapphire terraces start to coalesce and form higher steps of 1 nm. A MoS_2 nucleation chain is formed at these steps. The images show an area of 1 μm × 1 μm. All scale bars have length of 0.2 μm. The blue line in the first image indicates the substrate flat orientation (Color figure online).

Figure 1b shows the surfaces of a sample deposited with an identical MoS_2 growth process but after a prebake of the sapphire substrate at 1050°C in N_2 atmosphere for 15 min. While the nucleation density strongly decreased, the size of the MoS_2 crystals increased. The typical triangular structure can now be clearly resolved by SEM. This change in nucleation density can most likely be explained by the improved substrate surface, which leads to increased diffusion length of adatoms during growth, hence increasing the probability that growth species chemisorb at existing nucleation sites rather than form new ones. This effect can be enhanced either by increasing the prebake temperature or by extending the prebake duration. The prebake performed in H_2 atmosphere showed a quite similar trend. The results of the different prebake processes are summarized in Fig. 2. The nucleation site density for each sample was extracted from three different SEM images using the image processing program ImageJ.[18] It can be seen that the best results were obtained after a prebake at 1050°C in H_2 for 15 min (Fig. 1c), under which conditions the nucleation density was reduced from 550 nuclei/μm^2 without a prebake to 100 nuclei/μm^2. Further increase of the prebake temperature in H_2 to 1100°C led to degradation of the sapphire substrate. The sapphire terraces coalesced and formed wider terraces with higher steps of about 1.4 nm (as measured by AFM, Fig. S1 in Electronic Supplementary Material). One of those merging steps can be seen in Fig. 1d, appearing to be a preferred nucleation site for 2D MoS_2 resulting in j-shaped nucleation chains. The nucleation density of this sample could not be extracted by ImageJ, since the nuclei coalesced along the sapphire step into one large structure; hence, it is not included in Fig. 2. For homogeneous nucleation density, the prebake temperature of 1100°C is too high, even more so as coalescence of two MoS_2 crystals over the 1 nm step height is considered unlikely.

Besides the reduction in nucleation density, the H_2 prebake also prevented formation of parasitic carbonaceous film during growth, as revealed by Raman spectroscopy and discussed below. Such a carbonaceous film was observed on sapphire substrates without or with N_2 prebake for extended growth times ($>$ 10 h). In such cases, the MoS_2 crystals did not exceed size of 50 nm, but appeared embedded in a continuous film. Obviously, further growth of the crystals was hampered by this carbonaceous film (Fig. S2 in Electronic Supplementary Material). The height of this film could be measured by AFM and was found to be about 0.6 nm. Raman measurements on these samples revealed strong signals at 1360 cm^{-1} and 1600 cm^{-1} (Fig. 3), which can be attributed to the D and G Raman modes of carbon.[19] A similar carbon layer was reported by Zhang et al.[20] during growth of WSe_2. They ascribed this film to deposition of hydrocarbon groups from the dimethyl selenide

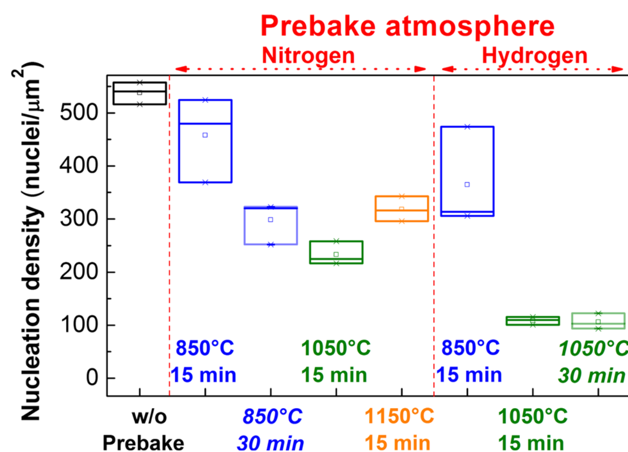

Fig. 2. Boxplot of nucleation density for samples deposited after different prebakes. Values extracted from three different SEM images using the image processing program ImageJ. The three horizontal bars in a box indicate the minimum, median, and maximum of the nucleation density, while the small square indicates the average value.

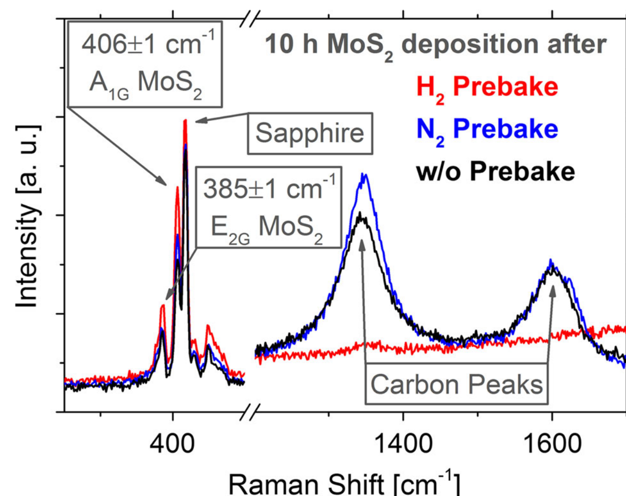

Fig. 3. Raman spectroscopy measurements of three samples deposited at 845°C and 30 hPa for 10 h after different prebakes. The "H_2 prebake" is the optimum prebake at 1050°C in H_2 for 15 min, and the sample exhibits no carbon signals. The "N_2 prebake" was performed at 1050°C in N_2 for 15 min. The laser of the Raman measurement setup had a wavelength of 532 nm.

precursor and therefore changed the S precursor to H_2Se. To clarify the origin of the carbonaceous film on our samples, single-source MOVPE processes, with either DTBS only or MCO only, were performed. The resulting Raman spectra (Fig. S3 in Electronic Supplementary Material) clearly indicated that DTBS was the source of the carbon-containing film in our MOVPE process. However, formation of a carbonaceous film could also be prevented, or at least strongly reduced, by using the prebake process in H_2, as shown in Fig. 3. This result shows the importance of the surface pretreatment for the later MoS_2 growth, as the formation of the carbonaceous film clearly depended on the substrate surface properties.

In the second growth series, the influence of the reactor pressure on the nucleation process was investigated to reduce the nucleation density. Figure 4a displays the surface of a MoS_2 sample deposited at 845°C and 30 hPa for 6 h after a H_2 prebake. The thermodynamically favored triangular crystal structure of MoS_2 can be observed. The average edge length of the domains was about 67 nm with nucleation density of 75 nuclei/μm^2. On increasing the reactor pressure to 60 hPa and 100 hPa (Fig. 4b), the nucleation density decreased to 57 nuclei/μm^2 and 50 nuclei/μm^2, respectively. Simultaneously, the average edge length increased to 79 nm and 86 nm. Comparing the overall coverage of the sample surfaces extracted via ImageJ, the MoS_2 coverage increased from 14% (30 hPa) to 17% (60 hPa) and 21% (100 hPa). This linear increase of the coverage suggests that the growth rate generally increased at higher pressures, most likely due to higher partial pressure and greater sticking efficiency of the growth species. In Fig. 4b, the regular orientation of MoS_2 domains on sapphire can be seen. The triangles point to either the top right or bottom left of the image. For reactor pressure above 100 hPa, the morphology of the domains appeared to change from triangular to hexagonal shape in SEM. This change was also confirmed by AFM measurements, as shown in Fig. 4d for the sample deposited at 400 hPa.

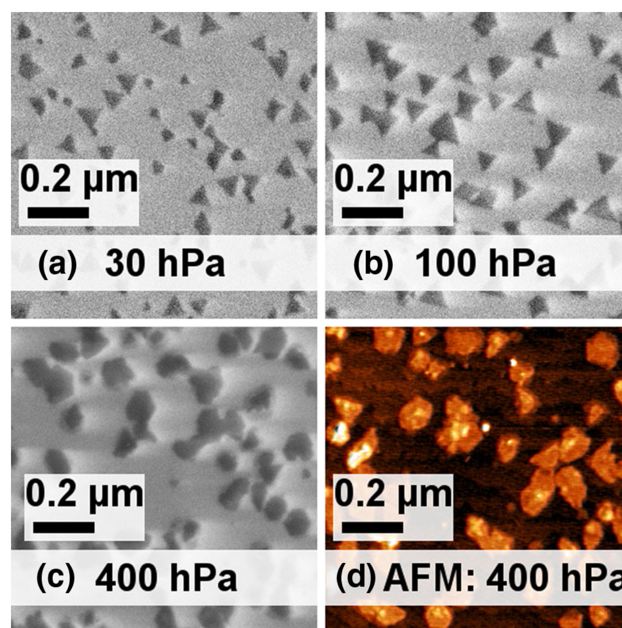

Fig. 4. SEM images of MoS_2 samples deposited at 30 hPa (a), 100 hPa (b), and 400 hPa (c). Growth was performed after the optimum H_2 prebake at 1050°C and at 845°C for 6 h. To confirm the hexagonal morphology of the sample deposited at 400 hPa, an additional AFM image is shown in (d). The height of the hexagonal domains is 0.9 nm to 1.1 nm. The images show an area of 1 $\mu m \times 1$ μm. All scale bars have length of 0.2 μm.

For further characterization, the samples were measured via Raman spectroscopy; the spectra are displayed in Fig. 5. The spectra of the samples grown at higher pressures are vertically shifted to allow distinction of the different measurements. Nevertheless, it is still noticeable that the intensities of the MoS_2 peaks at 385 cm^{-1} and 406 cm^{-1} increased relative to the sapphire peak due to the higher overall coverage at higher reactor pressure. Starting from the sample deposited at 100 hPa, the measurements also exhibited increasing signals at 1360 cm^{-1} and 1600 cm^{-1} for higher growth pressure, indicating carbon contamination. In contrast to the previous experiments without prebake, a parasitic carbonaceous film could not be identified in SEM or AFM images. The hexagonal structures in Fig. 4d are 0.9 nm to 1.1 nm high and thus thicker than a monolayer of MoS_2. Most likely, the carbonaceous film is below the MoS_2 crystallites, which would also explain their different morphology. Transmission electron microscopy (TEM) measurements will be necessary to verify this hypothesis.

In the final growth series, the impact of temperature on the lateral growth of MoS_2 was investigated with the goal of enhancing the size of the MoS_2 crystallites. The temperature dependence of the MoS_2 nucleation is shown in the Electronic Supplementary Material. Here, a strong decrease of the nucleation density was observed with increasing growth temperature (Figs. S4, S5). This trend is consistent with thermodynamical calculations of the nucleation process in literature.[21] For characterization of the lateral growth, the temperature was varied between 670°C and 1070°C in a 6-h growth step after a nucleation step at 845°C and 30 hPa for 4 h. Figure 6a shows the sample deposited at 670°C in the second growth phase. The larger triangular crystals are MoS_2 domains, which formed in the first growth phase and grew in size during the second phase. Additionally, a large number of smaller nuclei were observed on the surface, appearing to agglomerate preferentially around the larger crystals. These nuclei were formed in the second growth step. Such agglomeration around already existing MoS_2 may be explained by a catalytic behavior of the MoS_2 surface during the decomposition reactions of the precursors. Another possibility is that edge atoms of the existing nuclei can desorb, diffuse a certain distance (limited by the diffusion length) on the surface, and form new nucleation sites. In this scenario, existing domains function as parasitic sources. Such smaller nuclei around domains from the first growth phase were also observed at 750°C and 785°C. However, their density decreased with increasing growth temperature, most likely since the diffusion length of the growth species increased and the growth species could adsorb at existing nucleation sites. At 785°C, 845°C, and 905°C, the nucleation density and average domain size remained nearly constant. The surface of the sample deposited at 785°C is shown exemplarily in Fig. 6b. This indicates that the lateral growth was independent of the temperature in this range, thus a transport-limited growth regime was reached. This growth regime is preferred in MOVPE, since the processes can be easily controlled via the precursor flows. Increasing the temperature further to 950°C led to a reduction in the average nucleation size (Fig. 6c). The domains were only slightly larger than those after the first growth phase. Higher temperatures (1020°C and 1070°C) resulted in a complete change of morphology. The Raman measurement results are summarized in Fig. 7, indicating that the modified morphology at high temperatures was due to exclusive deposition of a carbonaceous film. The MoS_2 peaks disappeared for these samples. Overall, carbon contamination appeared for growth temperatures above 960°C, limiting the optimum growth temperature to between 785°C and 905°C.

Finally, the optimum growth conditions for reduced carbon contamination (845°C and 30 hPa) were used in extended growth processes. The growth time was increased stepwise to 20 h. However, a fully coalesced film was not achieved. The maximum overall coverage was about 70%, revealing a very low growth rate. In future, it will be necessary to investigate and optimize the lateral growth in more detail to reduce the growth time.

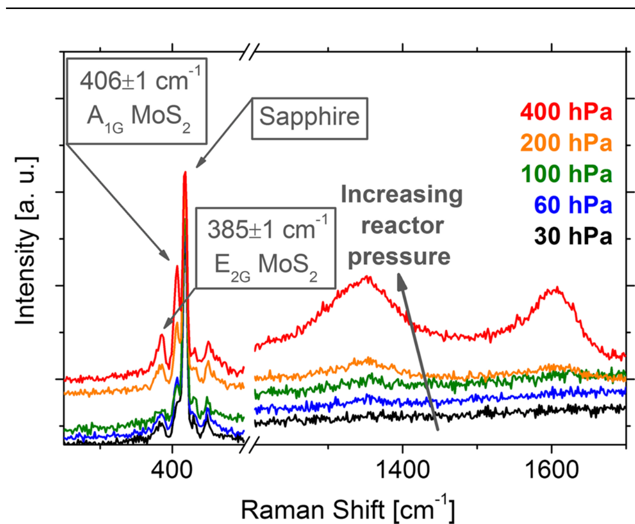

Fig. 5. Raman spectroscopy measurements of samples deposited at different reactor pressures and at 845°C after the optimum H_2 prebake at 1050°C. At higher reactor pressure, the intensity of the MoS_2 signals increased relative to the sapphire signal due to the higher overall coverage of the sample. However, also the carbon signals increased above 100 hPa, due to enhanced carbon incorporation or deposition. The data points for samples grown at higher pressures are vertically shifted (upwards) to allow distinction of the different measurements (grey arrow). The laser of the Raman measurement setup had a wavelength of 532 nm.

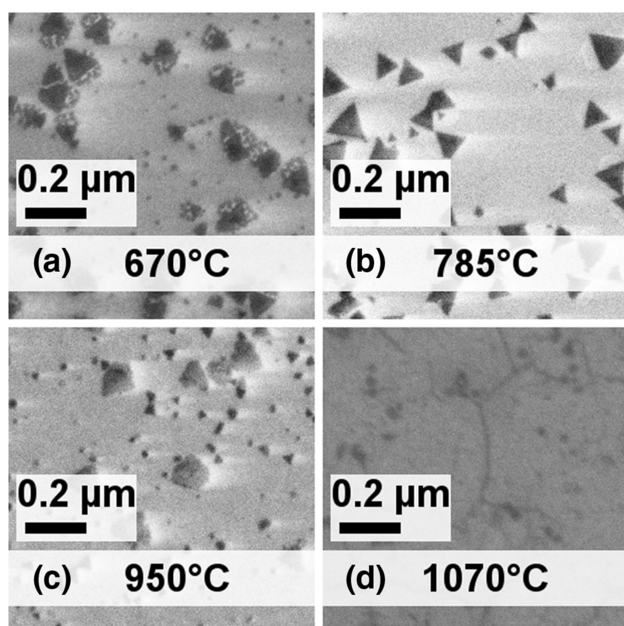

Fig. 6. SEM images of 2D MoS_2 nucleation sites deposited at 670°C (a), 785°C (b), 950°C (c), and 1070°C (d). The reactor pressure was set to 30 hPa. Prior to growth, the optimum H_2 prebake at 1050°C was performed. The images show an area of 1 μm × 1 μm. All scale bars have length of 0.2 μm.

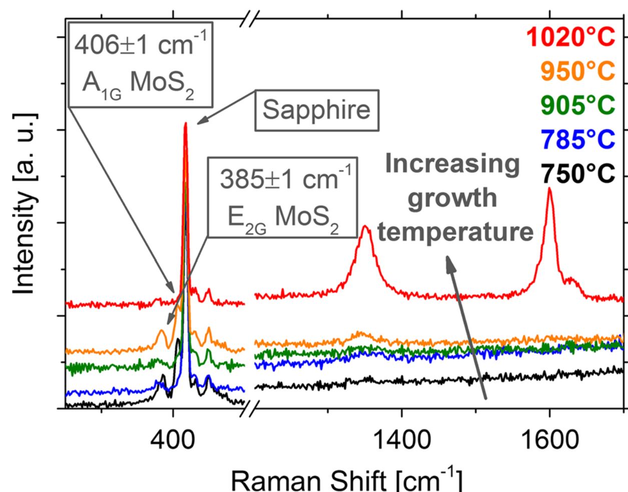

Fig. 7. Raman spectroscopy measurements of samples deposited at different growth temperatures and at 30 hPa after the optimum H_2 prebake at 1050°C. At temperatures above 950°C, the intensity of the carbon signals at 1380 cm^{-1} and 1600 cm^{-1} increased due to enhanced carbon incorporation or deposition. For growth temperature of 1020°C, the MoS_2 Raman peaks could not be detected. The data points of samples grown at higher temperatures are vertically shifted (upwards) to allow distinction of the different measurements (grey arrow). The laser of the Raman measurement setup had a wavelength of 532 nm.

CONCLUSIONS

The influence of different growth conditions during MOVPE of 2D MoS_2 was investigated. The results show that nucleation of MoS_2 took place at terraces on the sapphire substrate. Furthermore, the impact of different prebake processes on later MoS_2 growth was analyzed. It was shown that a prebake of the substrate could reduce the nucleation density and thus increase the average edge size of the MoS_2 crystals. The best results were obtained after a prebake at 1050°C in pure H_2 atmosphere for 15 min, which decreased the nucleation density fivefold to 100 nuclei/μm^2. Additionally, the optimal H_2 prebake prevented, or at least strongly inhibited, the formation of a parasitic carbonaceous film, which could otherwise hinder lateral growth of MoS_2. In a second growth series, it was shown that the nucleation density further decreased for deposition at higher pressure, while the average edge size of the crystals increased. This effect does not only originate from redistribution of the same amount of growth species at fewer nucleation sites, but is also accompanied by higher total coverage of the surface. However, the morphology of the domains changed from triangular to hexagonal at pressure above 100 hPa, most likely due to formation of a carbonaceous film below the MoS_2. Finally, in a third growth series, the optimum growth temperature was identified to lie between 785°C and 905°C. Lower temperatures resulted in very high nucleation density, while higher temperatures again led to deposition of a parasitic carbonaceous film.

Nevertheless, the origin of the carbon signals in Raman measurements is still not fully understood. In the future, we want to localize the carbon contamination in samples deposited at higher temperatures or pressures. TEM images could potentially reveal whether the carbon is located below, in, or/and on top of the MoS_2 crystals. Additionally, it will be interesting to investigate its influence on the lateral growth in more detail.

ELECTRONIC SUPPLEMENTARY MATERIAL

The online version of this article (https://doi.org/10.1007/s11664-017-5937-3) contains supplementary material, which is available to authorized users.

REFERENCES

1. I.G. Lezama, A. Arora, A. Ubaldini, C. Barreteau, E. Giannini, M. Potemski, and A.F. Morpurgo, *Nano Lett.* 15, 2336 (2015).
2. Y. Ding, Y. Wang, J. Ni, L. Shi, S. Shi, and W. Tang, *Phys. B* 406, 2254 (2011).
3. J.A. Wilson and A.D. Yoffe, *Adv. Phys.* 18, 193 (1969).
4. D. Akinwande, C. J. Brennan, J. S. Bunch, P. Egberts, J. R. Felts, H. Gao, R. Huang, J.-S. Kim, T. Li, Y. Li, K. M. Liechti, N. Lu, H. S. Park, E. J. Reed, P. Wang, B. I. Yakobson, T. Zhang, Y.-W. Zhang, Y. Zhou, and Y. Zhu, *Extreme Mech. Lett.* 13, 42 (2017).
5. E.M. Vogel and J.A. Robinson, *MRS Bull.* 40, 558 (2015).

6. M. Marx, S. Nordmann, J. Knoch, C. Franzen, C. Stampfer, D. Andrzejewski, T. Kümmell, G. Bacher, M. Heuken, H. Kalisch, and A. Vescan, *J. Cryst. Growth* 464, 100 (2017).
7. S.M. Eichfeld, V.O. Colon, Y. Nie, K. Cho, and J.A. Robinson, *2D Mater.* 3, 025015 (2016).
8. K. Kang, S. Xie, L. Huang, Y. Han, P.Y. Huang, K.F. Mak, C.-J. Kim, D. Muller, and J. Park, *Nature* 520, 656 (2015).
9. L. Liu, H. Qiu, J. Wang, G. Xu, and L. Jiao, *Nanoscale* 8, 4486 (2016).
10. T. Kim, J. Mun, H. Park, D. Joung, M. Diware, W. Chegal, J. Park, S.-H. Jeong, and S.-W. Kang, *Nanotechnology* 28, 18LT01 (2017).
11. T. Ohta, F. Cicoira, P. Doppelt, L. Beitone, and P. Hoffmann, *Chem. Vap. Depos.* 7, 33 (2001).
12. P. O'Brien, M.A. Malik, M. Chuggaze, T. Trindale, J.R. Walsh, and A.C. Jones, *J. Cryst. Growth* 170, 23 (1997).
13. M.A. Malik, M. Afzaal, and P. O'Brien, *Chem. Rev.* 110, 4417 (2010).
14. K.D. Bronsema, J.L. de Boer, and F. Jellinek, *Z. Anorg. Allg. Chem.* 540, 15 (1986).
15. D. Dumcenco, D. Ovchinnikov, K. Marinov, P. Lazic, M. Gibertini, N. Marzari, O.L. Sanchez, Y.-C. Kung, D. Krasnozhon, M.-W. Chen, S. Bertolazzi, P. Gillet, A.F. i Morral, and A. Kis, *ACS Nano* 9, 4611 (2015).
16. S. Najmaei, M. Amani, M.L. Chin, Z. Liu, A.G. Birdwell, T.P. O'Regan, P.M. Ajayan, M. Dubey, and J. Lou, *ACS Nano* 8, 7930 (2014).
17. A.E. Muslimov, V.E. Asadchikov, A.V. Butashin, V.P. Vlasov, A.N. Deryabin, B.S. Roshchin, S.N. Sulyanov, and V.M. Kanevsky, *Crystallogr. Rep.* 61, 730 (2016).
18. https://imagej.net. Accessed 04 Aug 2017.
19. A.C. Ferrari and D.M. Basko, *Nat. Nanotechnol.* 8, 235 (2013).
20. X. Zhang, Z.Y. Al Balushi, F. Zhang, T.H. Choudhury, S.M. Eichfeld, N. Alem, T.N. Jackson, J.A. Robinson, and J.M. Redwing, *J. Electron. Mater.* 45, 6273 (2016).
21. M. Ohring, *Materials Science of Thin Films: Deposition and Structure*, 2nd ed. (San Diego: Academic, 2002), pp. 380–386.